Speed of sound data, derived perfect-gas heat capacities, and acoustic virial coefficients of a calibration standard natural gas mixture and its H$_2$-enriched blend

Daniel Lozano-Martín[a], David Vega-Maza[a], Alejandro Moreau[a], M. Carmen Martín[a], Dirk Tuma[b], José J. Segovia[a,*]

[a] TERMOCAL Research Group, Research Institute on Bioeconomy (BioEcoUVa), University of Valladolid, Escuela de Ingenierias Industriales, Paseo del Cauce 59, 47011 Valladolid, Spain.

[b] BAM Bundesanstalt für Materialforschung und -prüfung, D-12200 Berlin, Germany.

* Corresponding author e-mail: jose.segovia@eii.uva.es

Abstract

This work aims to address the technical aspects related to the thermodynamic characterization of natural gas mixtures blended with hydrogen for the introduction of alternative energy sources within the Power-to-Gas framework. For that purpose, new experimental speed of sound data are presented in the pressure range between (0.1 up to 13) MPa and at temperatures of (260, 273.16, 300, 325, and 350) K for two mixtures qualified as primary calibration standards: a 11 component synthetic natural gas mixture (11 M), and another low-calorific H$_2$-enriched natural gas mixture with a nominal molar percentage $x_{H_2} = 3$ %. Measurements have been gathered using a spherical acoustic resonator with an experimental expanded ($k = 2$) uncertainty better than 200 parts in 10^6 (0.02 %) in the speed of sound. The heat capacity ratio as perfect-gas γ^{pg}, the molar heat capacity as perfect-gas $C_{p,m}^{pg}$, and the second β_a and third γ_a acoustic virial coefficients are derived from the speed of sound values. All the results are compared with the reference mixture models for natural gas-like mixtures, the AGA8-DC92 EoS and the GERG-2008 EoS, with special attention to the impact of hydrogen on those properties. Data are found to be mostly consistent within the model uncertainty in the 11 M synthetic mixture as expected, but in the limit of the model uncertainty at the highest measuring pressures for the hydrogen-enriched mixture.

1. Introduction.

The quest for a sustainable and carbon dioxide-free energy new economy paradigm has become a priority. One of the proposals with promising potential for a cost-effective transition from our current highly energy-dependent model is the, so called, Power-to-Gas [1,2]. The essence of the Power-to-Gas technique is the storage and transport of energy in the form of pressurized hydrogen by blending it with the natural gas so that the existing natural gas network can be used without the need for a separate infrastructure [3]. Provided that hydrogen is produced by: (a) electrolysers powered with the surplus of electric energy from renewable sources, like wind, solar, hydraulic or nuclear plants; (b) the steam reforming of natural gas or gasification and reforming of coal, oil, and biomass with carbon capture utilization and storage technologies, there is a reduction in net carbon dioxide emissions [4]. Hydrogen can be used either pure or blended with natural gas as a fuel, as feedstock for methanation [5], or for production of chemical and other fuels production after separation.

Implementing Power-to-Gas projects requires models that correctly describe the thermodynamic behavior of natural gas mixtures enriched with hydrogen. The aim of this research is to improve the accuracy and assess uncertainties of the equations of state that model the thermodynamic behavior of those mixtures, by virtue of the discussion of the differences between the experimental speed of sound and its derived heat capacity and the models' predictions on a 11 component synthetic natural gas (11 M) and a H_2-enriched mixture for wide ranges of temperature and pressure. Additionally, accurate measurements of the speed of sound are of interest in the monitoring of composition changes in a gas line [6,7], the design of pipelines to prevent propagation of fractures after decompression [8,9], the calibration of sonic nozzles for gas flow metering [10], or even the implementation of supersonic separators [11,12].

Although there is extensive literature about the speed of sound in multicomponent natural gas-like mixtures [13–18], none of these investigations deals with mixtures containing hydrogen, the

objective of this research. Following a previous work reporting accurate experimental (p, ρ, T) data with exactly these two gas mixtures [19], we have measured speeds of sound and compared them with the corresponding calculations obtained from the reference thermodynamic mixture models most widely used in the industry, namely the AGA8-DC92 [20,21] and GERG-2008 [22,23], respectively. To accomplish this task, measurements were carried out in the gas and supercritical (p,T) states depicted in Figure 1, extending at pressures up to 13 MPa at five temperature between 260 K and 350 K. Speed of sound was determined using the most precise experimental technique, the spherical acoustic resonator [24].
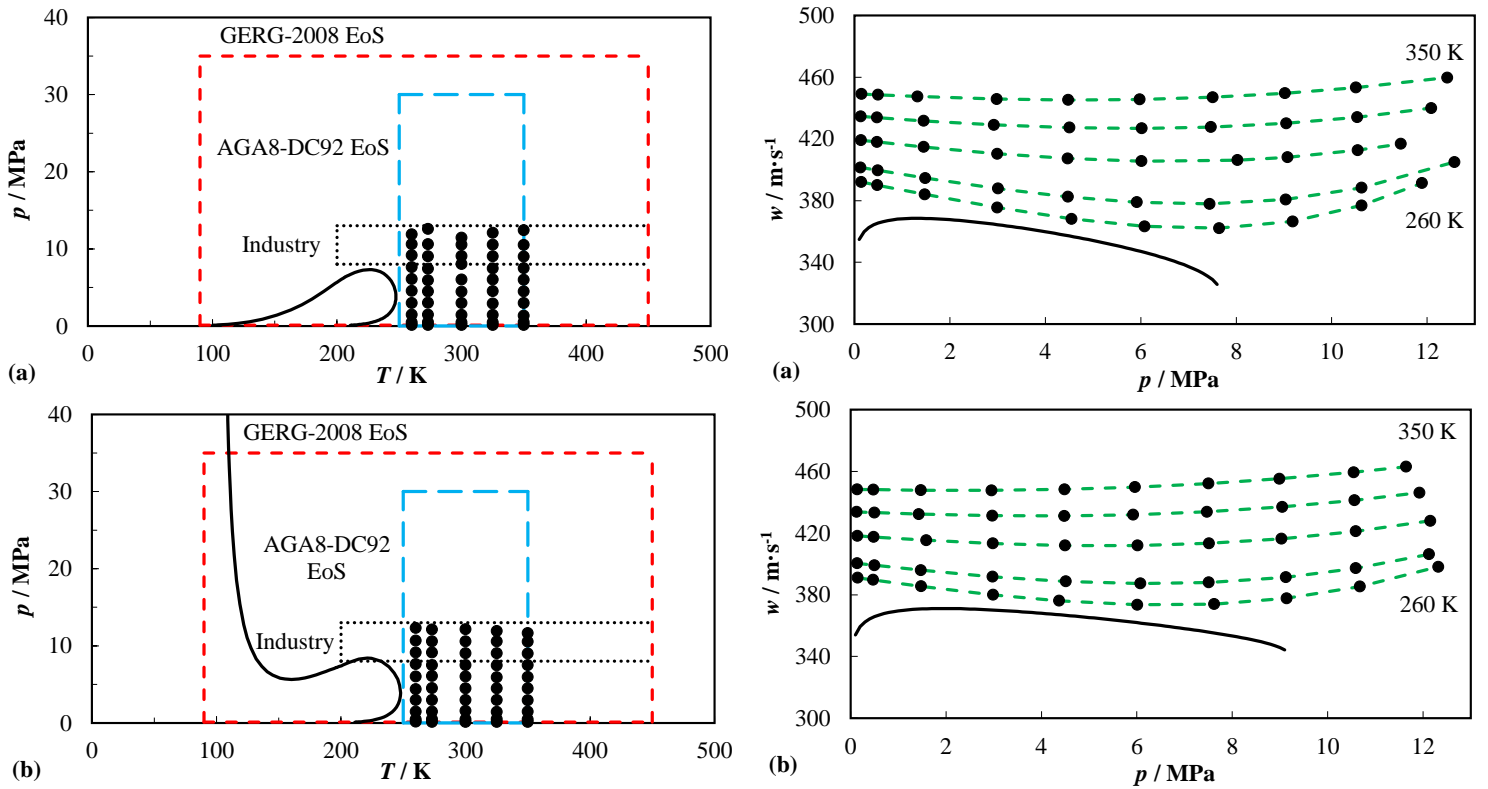
Figure 1. (p, T) and (w, p) phase diagrams showing the experimental points measured (•) and the calculated phase envelope (solid line) using the GERG-2008 EoS [22,23] for: a) the 11 component synthetic natural gas mixture (11 M) and b) the H_2-enriched natural gas mixture. The marked temperature and pressure ranges represent the normal range of application of the AGA8-DC92 EoS [20,21] (blue long dashed line) and the GERG-2008 EoS [22,23] (red short dashed line), respectively, and the area of interest for the gas industry (black dotted line). The green dashed lines serve as a guide for the eye.

2. Materials and methods.

2.1 Mixtures.

The two gas mixtures studied in this work were prepared by the Federal Institute for Materials Research and Testing (Bundesanstalt für Materialforschung und -prüfung, BAM) in Germany using pure gases with the specifications given in Table 1.

Table 1. Purity, supplier, molar mass, and critical parameters of the pure components used for the preparation of the two gas mixtures at BAM.

	Supplier	CAS-number	Purity / mol-%	M / g·mol^{-1}	Critical parameters[a]	
					T_c / K	p_c / MPa
Methane	Linde AG	74-82-8	$\geq$ 99.9995	16.043	190.564	4.5992
Ethane	Matheson Tri-Gas	74-84-0	$\geq$ 99.999	30.069	305.322	4.8722
Propane	Scott Specialty Gases BV	74-98-6	$\geq$ 99.999	44.096	369.890	4.2512
Butane	Scott UK	106-97-8	$\geq$ 99.95	58.122	425.125	3.7960
Isobutane	Scott Specialty Gases	75-28-5	$\geq$ 99.98	58.122	407.810	3.6290
Pentane	Sigma-Aldrich Chemie	109-66-0	$\geq$ 99.7	72.149	469.700	3.3675
Isopentane	Sigma-Aldrich Chemie	78-78-4	$\geq$ 99.7	72.149	460.350	3.3780
Neopentane	Linde AG	463-82-1	$\geq$ 99.0	72.149	433.740	3.1960
Hexane	Sigma-Aldrich Chemie	110-54-3	$\geq$ 99.7	86.175	507.820	3.0441
Carbon dioxide	Air Liquide AG	124-38-9	$\geq$ 99.9995	44.010	304.128	7.3773
Nitrogen	Linde AG	7727-37-9	$\geq$ 99.9995	28.014	126.192	3.3958
Oxygen	Westfalen AG	7782-44-7	$\geq$ 99.9999	31.999	154.581	5.0430
Helium	Linde AG	7440-59-7	$\geq$ 99.9995	4.003	5.195	0.2283
Hydrogen	Linde AG	1333-74-0	$\geq$ 99.9999	2.016	33.145	1.2964

[a] Critical parameters were obtained by using the default equation for each substance in REFPROP 10.0 software [25].

The first mixture matches a pipeline-quality rich natural gas composed of 11 components and denoted as 11 M synthetic natural gas, whereas the second mixture resembles a low-calorific 12

components natural gas blended with hydrogen denoted as H_2-enriched natural gas. The normalized compositions and corresponding expanded ($k = 2$) uncertainties of both mixtures are reported in Table 2. More detailed description of the filling steps, premixture realizations, and gas chromatographic validations of the gravimetric procedure used for the preparation of the mixtures (according to ISO 6142-1 [26]) can be followed on the Experimental section and Appendix A of our previous work [19].

Remark that the H_2-enriched natural gas mixture is not a real blend of the 11 M synthetic mixture (the composition of several components, such as ethane, propane, nitrogen, and carbon dioxide, is rather different). The 11 M mixture is a primary certificate standard mixture proposed by the Physical-Technical Federal Institute (Physikalisch-Technische Bundesanstalt, PTB), whereas the H_2-enriched natural gas mixture is a mixture proposed by the Consultative Committee for Amount of Substance (Comité consultative pour la quantité de matière, CCQM) for key comparisons.

Table 2. Normalized molar composition x_i and expanded ($k = 2$) uncertainty $U(x_i)$ of the two natural gas mixtures studied in this work.

Components	CAS-number	11 M synthetic natural gas[a]		H_2-enriched natural gas[b]	
		$10^2 \cdot x_i$ / mol·mol^{-1}	$10^2 \cdot U(x_i)$ / mol·mol^{-1}	$10^2 \cdot x_i$ / mol·mol^{-1}	$10^2 \cdot U(x_i)$ / mol·mol^{-1}
Methane	74-82-8	87.6637	0.0035	78.8212	0.0038
Ethane	74-84-0	4.22521	0.00046	0.75736	0.00016
Propane	74-98-6	1.0490	0.0021	0.297078	0.000089
Butane	106-97-8	0.21265	0.00010	0.200439	0.000098
Isobutane	75-28-5	0.210325	0.000084	0.197954	0.000035
Pentane	109-66-0	0.051829	0.000027	0.050134	0.000021
Isopentane	78-78-4	0.052184	0.000027	0.049928	0.000021
Neopentane	463-82-1			0.049615	0.000031
Hexane	110-54-3	0.052567	0.000024	0.050708	0.000019
Carbon dioxide	124-38-9	1.62285	0.00030	4.00108	0.00028
Nitrogen	7727-37-9	4.32170	0.00078	12.01783	0.00077

Oxygen	7782-44-7	0.53801	0.00011		
Helium	7440-59-7			0.49690	0.00030
Hydrogen	1333-74-0			3.0097	0.0013

[a] BAM bottle no./BAM mixture label: C49358-090825/BAM-G420.

[b] BAM bottle no./BAM mixture label: 8099-160905/CCQM-K118.

Note that the reported gravimetric compositions [19] include traces of existing impurities originating from the pure components as well, which are not specifically listed in Table 2 presented in this work. However, their contribution was accounted in the mole fraction uncertainty given in Table 2. In addition, neopentane (2,2-dimethylpropane) is considered neither in the AGA8-DC92 EoS [20,21] nor in the GERG-2008 EoS [22,23]. Hence, it must be treated as a trace component and its composition added to the composition of n-pentane as indicated in ISO 20765-2 [27], whereby the mixture model is still valid should the composition of all of these trace components not exceed a mole percentage of 0.05, as it is the case here.

Finally, the two mixtures were homogenized by heating and rolling at BAM before taking the measurements.

2.2 Experimental setup.

The experimental apparatus is the same as described before [28,29], thus a brief description is given here for completeness. The main part is the acoustic resonant cavity made with a spherical shape within tolerances better than 1 μm in 321 austenitic stainless steel. Two hollow hemispheres were welded by electron beam. It was designed to be a pressure-tight shell of 268 cm^3 with a wall of a thickness $b = 12.5$ mm and a nominal internal radius $a = 40$ mm. Dependence of the latter $a(p,T)$ with pressure and temperature has been determined previously [29] by speed of sound measurements in argon, a gas with an established equation of state [30].

Four ports are opened in the cavity wall. Two ports with 1.5 mm radius in the northern hemisphere form an angle of 45° with the north pole to accommodate the plugs where the acoustic transducers (source and detector) are placed. The other two ports with a radius $r_0 = 0.8$ mm are to provide access to the inlet gas duct of length $L_1 = 2.3$ m and a blind duct of length $L_2 = 0.035$ m, respectively, the latter used for measuring the speed of sound with gas flow but deactivated during

this work. They are located in the north and south poles, respectively. This cavity is located inside a vacuum-tight vessel which in turn is submerged in a Dewar vessel filled with ethanol and cooled by a stirred thermal bath at $T = -22.5°C$. Three band resistors around the copper block that clamp the north pole of the cavity, the side and the bottom of the shell heat the resonator to the desired experimental temperature which is controlled by a PID (proportional-integral-derivative) loop, with a thermal stability in the order of 1 mK during the entire experimental runs.

A 40 V peak-to-peak signal amplified up to 180 V is sent from the wave generator (3225B function generator, HP) across a set of electrical feed-throughs in the top plate of the vessel to the source capacitance-type acoustic transducer, constructed by a thin polyamide film of 12 μm thickness and gold-plated in the side facing the interior of the acoustic cavity. It generates an acoustic signal up to 20 mPa which is detected by an equal transducer at twice the driven frequency f, plugged to a high-input impedance amplifier in order to operate at constant charge. The detected signal is driven by triaxial cables across the feed-throughs to a lock-In amplifier (SR850 DSP Lock-In, SRS) working at differential mode and phase-locked with the wave synthesizer. The signal is then decomposed to the in-phase u and quadrature v components and fitted to a Lorentzian function:

$$u + \mathrm{i}v = \frac{A^*}{\left(F^2 - f^2\right)} + B^* + C^* f \tag{1}$$

where A^* is a term proportional to the amplitude of the acoustic field inside the resonator and the sensitivity of the detector acoustic transducer, B^* and C^* are complex terms that account for the constant and linear background level, and $F = f_{0n} + \mathrm{i}g_{0n}$ stands for the complex resonance frequency with f_{0n} and g_{0n} equal to the experimental resonance frequency and halfwidth of the radial non-degenerate $(l = 0, n)$ mode, respectively.

The thermodynamic state is determined by the mean of the temperature readings from two standard platinum reference thermometers (25.5 Ω SPRT 162D, Rosemount) located in the northern and souther hemispheres of the acoustic cavity and monitored by an AC resistance bridge (F18 automatic bridge, ASL). This system has been calibrated in our accredited facilities on the ITS-90 [31] with an estimated expanded $(k = 2)$ uncertainty $U_{cal}(T) = 4$ mK. The pressure is

determined by two piezoelectric quartz transducers connected to the top of the inlet gas duct, which cover the ranges (0 to 2) MPa (Digiquartz 2003A-101-CE, Paroscientific) and (0 to 20) MPa (Digiquartz 43K-101, Paroscientific). They have also been calibrated against a dead-weight pneumatic balance in our laboratory. The estimated expanded ($k = 2$) uncertainty in pressure is $U_{cal} = (7.5 \cdot 10^{-5} \cdot (p/\text{MPa}) + 2 \cdot 10^{-4})$ MPa.

2.3 Measurement procedure and acoustic model.

Several consecutive repetitions of the resonance frequency f_{0n} and halfwidth g_{0n} of the first five purely radial acoustic modes (0,2), (0,3), (0,4), (0,5), and (0,6) are recorded at frequencies between (6.65 to 31.31) kHz, starting at the highest pressure of about 13 MPa down to approximately 0.1 MPa, upon reducing the pressure in 1.5-MPa steps and, when a stable temperature condition has been met at every pressure, typically after eight hours. Then, these measurements at each experimental $(p_i, T_{i,exp})$ state are corrected to specify them to the same reference temperature $T_{ref,}$ for every isotherm by multiplying them with the term $w(p_i, T_{ref})/w(p_i, T_{i,exp})$. Finally, from the mean of f_{0n} and g_{0n}, a speed of sound value w_{0n} is determined for every mode as shown in Equation (2):

$$w_{0n} = 2\pi a \frac{f_{0n} - \Delta f}{z_{0n}} \tag{2}$$

where a stands for the internal radius of the resonance cavity obtained as discussed above, z_{0n} stands for the n-th zero of the spherical Bessel first derivative of order $l = 0$, and Δf is the term that accounts for the sum of all frequency corrections due to the non-zero acoustic wall admittance and imperfect geometry of the cavity, respectively. The former case comprises the perturbations induced by the heat exchange in the thermal boundary layer [32], the coupling of the motion of the fluid and shell motion [33], and the presence of the source and detector acoustic transducers [24]. The latter case includes the perturbations due to the two gas ducts [34]. Other geometrical imperfections, such as slits in the equatorial joint or around the transducer plugs, are demonstrated to be negligible [32], with corrections less than 1 part in 10^6, especially for the radial acoustic modes, which are not sensitive to perturbations of the perfect sphericity on first order [35]. Standard models have been used to calculate these corrections, and the specific expressions of

every term have been reported elsewhere [36]. REFPROP 10.0 [25], computed the thermodynamic and transport properties of the gas mixtures required by these correction models using the GERG-2008 EoS [22,23]. The elastic and thermal properties of the stainless steel of the cavity wall were obtained from the correlations of [37] and [38,39], respectively, when required. The magnitude of the overall frequency perturbations $\Delta f/f$ that must be subtracted to the experimental frequencies f_{0n} ranges from (-130 to -250) parts in 10^6 for the (0,2) mode of the H_2-enriched mixture at $T = 260$ K up to (-50 to $+700$) parts in 10^6 for the (0,6) mode of the 11 M synthetic mixture at $T = 350$ K, which is in the order of the estimated expanded ($k = 2$) uncertainty $U_r(w_{exp}) \sim 200$ parts in 10^6 for the two mixtures as described below and, hence, not a negligible quantity.

The validity of the applied acoustic model is assessed by the extent of the relative dispersion of the speed of sound $\Delta w/w = (w_{0n} - <w>)/<w>$ from every mode w_{0n} around their mean $<w>$ and from the relative excess halfwidth $\Delta g/f$ for every acoustic mode:

$$\left.\frac{\Delta g}{f}\right|_{0n} = \frac{g_{0n} - \left(g_{th} + g_0 + g_{bulk}\right)}{f_{0n}} \tag{3}$$

where g_{th} is the contribution accounting for energy losses in the thermal boundary layer, g_0 is the term accounting for energy losses in the gas tubes, and g_{bulk} is the classical viscothermal dissipation in the bulk of the fluid. Figure 2 depicts $\Delta g/f$ and Figure 3 displays $\Delta w/w$ as a function of pressure for the two studied mixtures at the highest experimental isotherm $T = 350$ K. As can be seen from Figure 2, the relative excess halfwidths are always in the order of 30 parts in 10^6 for the modes (0,2), (0,3), and (0,4). By contrast, this magnitude is larger than the experimental expanded ($k = 2$) uncertainty $U_r(w_{exp}) \sim 200$ parts in 10^6 for the mode (0,5) at the lowest and highest pressures and for the mode (0,6) at all the pressures investigated.
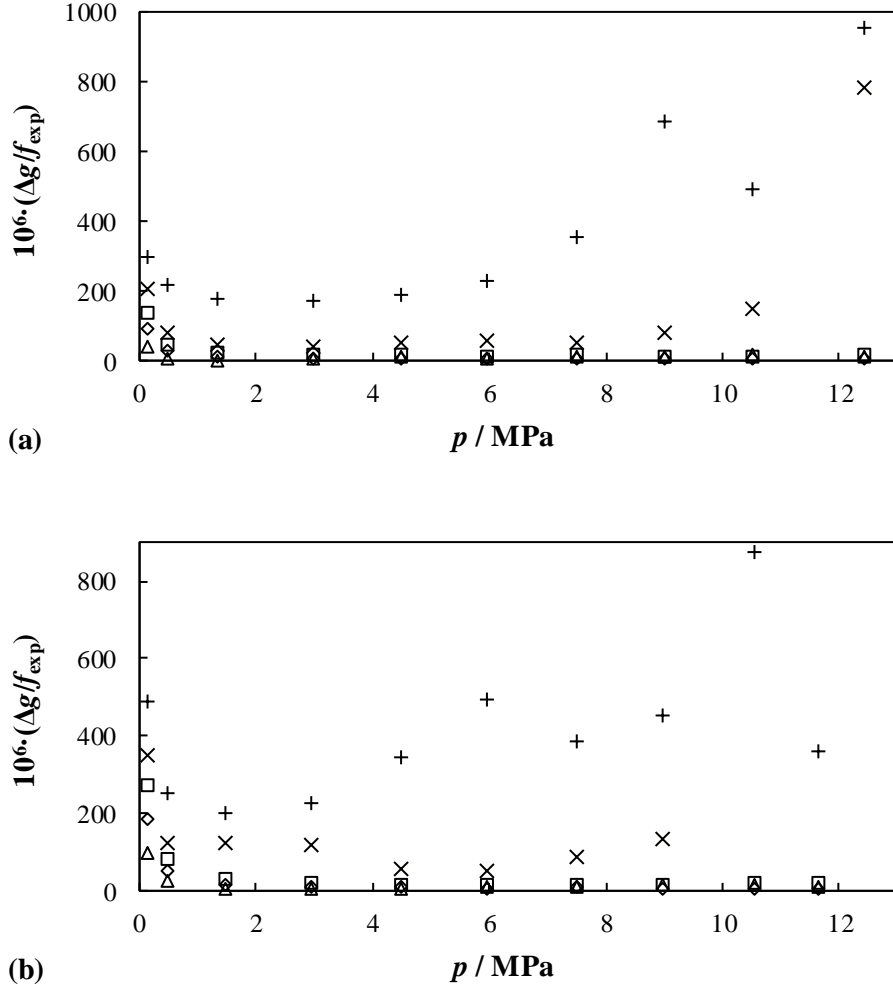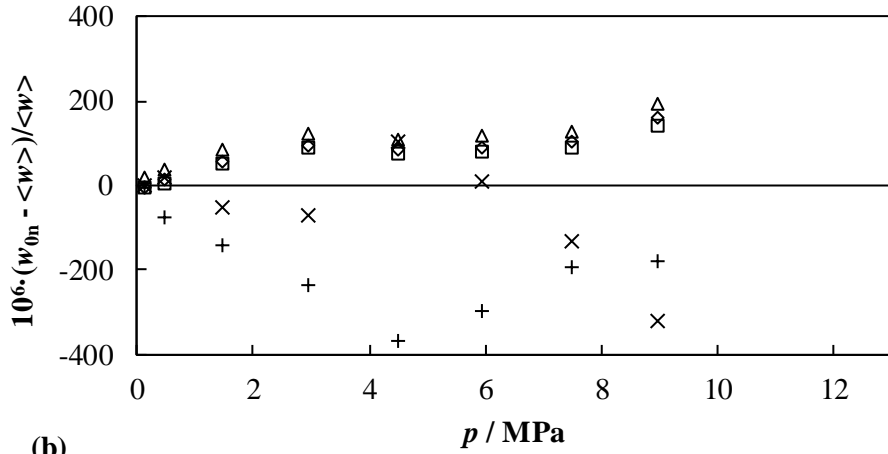
Figure 2. Relative excess halfwidths $\Delta g/f$ for: a) the 11 M synthetic natural gas and b) the H_2-enriched natural gas mixtures, at $T = 350$ K and modes $\triangle$ (0,2), $\diamondsuit$ (0,3), $\square$ (0,4), $\times$ (0,5), $+$ (0,6).

In addition, Figure 3 shows that modes (0,5) and (0,6) clearly disagree from the values of the other modes at several pressures, with speed of sound results outside the standard deviation of the mean of 15 parts in 10^6 for the modes (0,2), (0,3), and (0,4). Both reasons indicate that there are unknown imperfections of the used acoustic model, hence the model cannot perfectly reproduce the experimental situation inside the acoustic cavity. Similar results are found for the remaining isotherms. Thus, mode (0,6) at all the isotherms investigated, as well as mode (0,5) at (300, 325, and 350) K, have been skipped from the following calculations for the two studied mixtures.
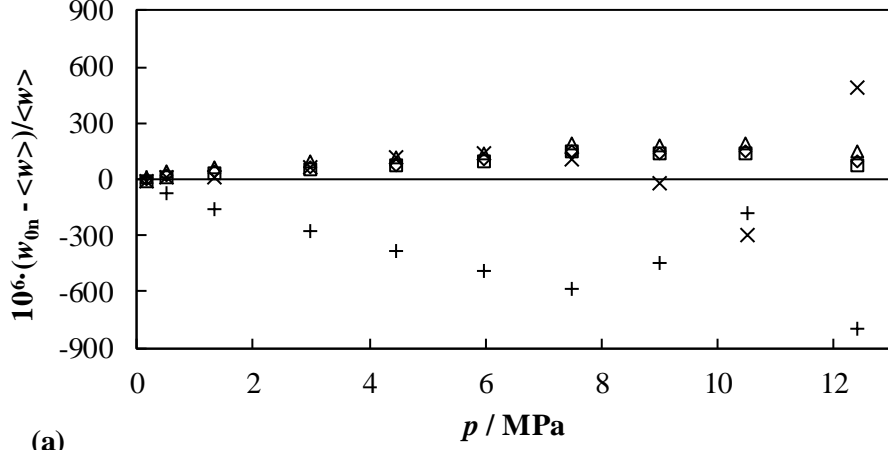
(a)

(b)

Figure 3. Relative dispersion of the speed of sound $\Delta w/w = (w_{0n} - <w>)/<w>$, where $<w>$ is the mean value from modes $(0,2)$ to $(0,6)$, as a function of pressure for: a) the 11 M synthetic natural gas and b) the H_2-enriched natural gas mixtures, at $T = 350$ K and modes $\triangle$ $(0,2)$, $\diamondsuit$ $(0,3)$, $\square$ $(0,4)$, $\times$ $(0,5)$, $+$ $(0,6)$.

3. Results and uncertainty.

One hundred experimental $w_{exp}(p,T,\bar{x})$ points have been measured at pressures p from $(0.1$ up to $13)$ MPa and temperatures $T = (260, 273.16, 300, 325,$ and $350)$ K. Tables 3 and 4 show the data sets for the 11 M synthetic natural gas and the H_2-enriched natural gas, respectively. Each point reports the mean of the speed of sounds determined from Equation (2) using the remaining radial $(0,n)$ resonance modes after rejection of those modes whose relative excess halfwidths $\Delta g_{0n}/f_{0n}$ are significantly larger and whose relative speed of sound dispersion $\Delta w/w$ clearly differs from the others, as discussed before.

11

Table 3. Speeds of sound $w_{exp}(p,T)$ for the 11 M synthetic natural gas mixture with their relative expanded ($k = 2$) uncertainty[a] and relative deviations $(w_{exp} − w_{EoS})/w_{EoS} = \Delta w/w_{EoS}$ from the speed of sound predicted by the AGA8-DC92 EoS [20,21] and the GERG-2008 EoS [22,23].

p / MPa	w_{exp} / m·s^{-1}	$10^6 \cdot (w_{exp} − w_{AGA})/w_{AGA}$	$10^6 \cdot (w_{exp} − w_{GERG})/w_{GERG}$	p / MPa	w_{exp} / m·s^{-1}	$10^6 \cdot (w_{exp} − w_{AGA})/w_{AGA}$	$10^6 \cdot (w_{exp} − w_{GERG})/w_{GERG}$
	$T = 260.00$ K				$T = 325.00$ K		
0.13876	392.127	−365	−418	0.12678	434.631	−131	−157
0.47800	390.049	−243	−328	0.46853	433.835	7	−59
1.47237	384.027	−122	−288	1.44685	431.680	192	20
2.98914	375.498	−40	−289	2.91962	429.075	394	68
4.54980	368.152	−60	−278	4.50284	427.322	590	112
6.07522	363.313	−204	−235	6.02004	426.847	776	166
7.63878	362.167	−375	−141	7.46732	427.656	950	227
9.18078	366.524	−477	−121	9.04454	430.111	1138	302
10.62418	376.894	−520	−341	10.53238	434.066	1315	383
11.89247	391.359	−559	−802	12.08749	439.989	1479	464
	$T = 273.16$ K				$T = 350.00$ K		
0.12548	401.437	−314	−353	0.14448	449.138	−85	−114
0.48846	399.604	−130	−210	0.49294	448.617	25	−47
1.48187	394.644	13	−174	1.31844	447.482	168	3
3.00368	387.794	178	−155	2.97716	445.865	388	56
4.47096	382.451	290	−134	4.47555	445.272	551	80
5.91417	378.958	362	−79	5.97484	445.613	703	101
7.43740	377.911	416	3	7.50472	447.030	864	142
9.03526	380.706	534	116	9.01878	449.576	1026	193
10.62452	388.354	675	149	10.50800	453.256	1184	257
12.57160	405.012	756	−17	12.41850	459.739	1361	342
	$T = 300.00$ K						

12

p / MPa	$w_{\exp}$ / m·s^{-1}	$10^6 \cdot (w_{\exp} - w_{\text{AGA}})/w_{\text{AGA}}$	$10^6 \cdot (w_{\exp} - w_{\text{GERG}})/w_{\text{GERG}}$
0.13664	419.154	−217	−250
0.47079	418.020	−31	−102
1.44929	414.762	147	−33
2.98746	410.383	339	−9
4.46523	407.305	518	26
6.01409	405.583	693	78
8.02558	406.238	926	183
9.07127	408.105	1050	240
10.54125	412.733	1240	329
11.44834	416.825	1350	382

[a] Expanded uncertainties ($k = 2$): $U(p) = (7.5 \cdot 10^{-5}\ (p/\text{Pa}) + 200)$ Pa; $U(T) = 4$ mK; $U_{\text{r}}(w) = 1.9 \cdot 10^{-4}$ m·s^{-1}/ m·s^{-1}.

Table 4. Speeds of sound $w_{\exp}(p,T)$ for the H$_2$-enriched natural gas mixture with their relative expanded ($k = 2$) uncertainty[a] and relative deviations $(w_{\exp} - w_{\text{EoS}})/w_{\text{EoS}}$ from the speed of sound predicted by the AGA8-DC92 EoS [20,21] and the GERG-2008 EoS [22,23].

p / MPa	$w_{\exp}$ / m·s^{-1}	$10^6 \cdot (w_{\exp} - w_{\text{AGA}})/w_{\text{AGA}}$	$10^6 \cdot (w_{\exp} - w_{\text{GERG}})/w_{\text{GERG}}$	p / MPa	$w_{\exp}$ / m·s^{-1}	$10^6 \cdot (w_{\exp} - w_{\text{AGA}})/w_{\text{AGA}}$	$10^6 \cdot (w_{\exp} - w_{\text{GERG}})/w_{\text{GERG}}$
	$T = 260.00$ K				$T = 325.00$ K		
0.14773	390.998	−562	−597	0.12437	433.728	−325	−336
0.47021	389.662	−295	−356	0.49608	433.303	−118	−161
1.47966	385.458	−101	−224	1.42737	432.303	104	−16
2.98774	379.964	87	−88	2.97052	431.250	329	107
4.37248	376.083	176	14	4.47759	431.088	494	207
6.00833	373.541	284	201	5.92270	431.850	658	331
7.61769	373.929	425	377	7.47048	433.756	840	484
9.13792	377.666	694	454	9.04792	436.950	1042	654
10.67254	385.328	1050	290	10.56114	441.256	1234	794

12.31649	398.132	1368	−237	11.92213	446.191	1389	881
	T = 273.16 K				*T* = 350.00 K		
0.13451	400.369	−355	−409	0.13352	448.308	−372	−384
0.49849	399.129	−150	−235	0.47718	448.173	−145	−192
1.47309	395.917	91	−67	1.47412	447.782	80	−57
2.97290	391.704	289	46	2.95101	447.699	270	30
4.50887	388.664	450	167	4.48238	448.348	424	109
6.07316	387.302	612	326	5.96072	449.752	565	207
7.50730	387.979	794	492	7.50214	452.081	713	330
9.12321	391.385	1061	626	8.98999	455.210	868	467
10.58929	397.216	1344	621	10.54386	459.422	1026	601
12.12160	406.278	1615	447	11.64110	462.987	1135	688
	T = 300.00 K						
0.14344	418.185	−330	−349				
0.47956	417.502	−113	−160				
1.58308	415.333	111	−21				
2.97871	413.240	303	85				
4.49573	411.973	481	200				
6.01298	411.946	653	336				
7.51230	413.322	833	484				
9.02840	416.308	1053	647				
10.58955	421.186	1296	772				
12.14970	427.961	1516	815				

[a] Expanded uncertainties ($k = 2$): $U(p) = (7.5 \cdot 10^{-5}\ (p/\mathrm{Pa}) + 200)$ Pa; $U(T) = 4$ mK; $U_\mathrm{r}(w) = 1.8 \cdot 10^{-4}$ m·s^{-1}/ m·s^{-1}.

Tables 5 and 6 report the specified uncertainty contributions to the speed of sound of the 11 M synthetic natural gas mixture and the H_2-enriched natural gas mixture, respectively, as the average of the uncertainties of all speed of sound datasets. The square root of the sum of the squares of these components yields the overall relative expanded ($k = 2$) uncertainty of the speed of sound $U_r(w_{exp})$ of 190 parts in 10^6 (0.019 %) for the 11 M synthetic natural gas mixture and 180 parts in 10^6 (0.018 %) for the H_2-enriched natural gas mixture, respectively. As predicted, the most significant contribution to $U_r(w_{exp})$ is due to the geometrical characterization of the resonance cavity by means of speed of sound measurements in argon to determine the behavior of the internal cavity radius as function of the pressure and temperature $U(a)$, which amounts up to 170 parts in 10^6. Next is the contribution of the uncertainty of the composition of the gas mixtures $U(x_i)$ given in Table 2, which is lower than (70 and 50) parts in 10^6 for the 11 M synthetic mixture and the H_2-enriched mixture, respectively. Minor contributing terms are: (a) the adequateness of the acoustic model described above and quantified in the order of 10 parts in 10^6 as the standard deviation of the speed of sound from the different non-rejected modes $U(<w>)$; (b) the imperfect determination of the thermodynamic state, whose contribution is evaluated from the pressure uncertainty $U(p)$ as 3 part in 10^6 and from the temperature uncertainty $U(T)$ as 5 parts in 10^6; and (c) the error associated with the fitting of the recorded in-phase and quadrature acoustic signals to the Lorentzian shape function of Equation (1) $U(f_{0n})$, always below 1 part in 10^6. Detailed descriptions to calculate every part of the uncertainty have been given elsewhere [40,41].

Table 5. Uncertainty budget for the speed of sound measurements w_{exp} for the 11 M synthetic natural gas mixture. Unless otherwise specified, uncertainties are indicated with a coverage factor $k = 1$.

Source	Magnitude		Contribution to the speed of sound uncertainty, $10^6 \cdot u_r(w_{exp})$
	Calibration	0.002 K	
	Resolution	$7.2 \cdot 10^{-7}$ K	
Temperature	Repeatability	$5.9 \cdot 10^{-5}$ K	
	Gradient (across hemispheres)	$1.3 \cdot 10^{-3}$ K	
	Quadrature Sum	$2.5 \cdot 10^{-3}$ K	4.9

Source		Magnitude	Contribution
Pressure	Calibration	$(3.75 \cdot 10^{-5} \cdot p + 1 \cdot 10^{-4})$ MPa	
	Resolution	$2.9 \cdot 10^{-5}$ MPa	
	Repeatability	$1.2 \cdot 10^{-5}$ MPa	
	Quadrature Sum	$(1.1$ to $5.5) \cdot 10^{-4}$ MPa	2.8
Gas composition	Purity	$9.7 \cdot 10^{-7}$ kg/mol	
	Molar mass	$9.9 \cdot 10^{-7}$ kg/mol	
	Quadrature Sum	$1.4 \cdot 10^{-6}$ kg/mol	34
Radius from speed of sound in Ar	Temperature	$1.5 \cdot 10^{-9}$ m	
	Pressure	$1.6 \cdot 10^{-10}$ m	
	Gas Composition	$4.1 \cdot 10^{-9}$ m	
	Frequency fitting	$4.9 \cdot 10^{-7}$ m	
	Regression	$1.7 \cdot 10^{-6}$ m	
	Equation of State	$2.3 \cdot 10^{-6}$ m	
	Dispersion of modes	$2.9 \cdot 10^{-6}$ m	
	Quadrature Sum	$4.2 \cdot 10^{-6}$ m	88
Frequency fitting		$5.6 \cdot 10^{-3}$ Hz	0.51
Dispersion of modes		$5.7 \cdot 10^{-3}$ m$\cdot$s^{-1}	14
Quadrature Sum of all contributions to w_{exp}			95
$10^6 \cdot U_r(w_{exp})$ $(k = 2)$			190

Table 6. Uncertainty budget for the speed of sound measurements w_{exp} for the H_2-enriched natural gas mixture. Unless otherwise specified, uncertainties are indicated with a coverage factor $k = 1$.

Source	Magnitude		Contribution to the speed of sound uncertainty, $10^6 \cdot u_r(w_{exp})$
Temperature	Calibration	0.002 K	
	Resolution	$7.2 \cdot 10^{-7}$ K	
	Repeatability	$3.5 \cdot 10^{-5}$ K	
	Gradient (across hemispheres)	$1.0 \cdot 10^{-3}$ K	
	Quadrature Sum	$2.3 \cdot 10^{-3}$ K	4.4
Pressure	Calibration	$(3.75 \cdot 10^{-5} \cdot p + 1 \cdot 10^{-4})$ MPa	
	Resolution	$2.9 \cdot 10^{-5}$ MPa	
	Repeatability	$7.9 \cdot 10^{-6}$ MPa	
	Quadrature Sum	$(1.1$ to $5.5) \cdot 10^{-4}$ MPa	2.1

Gas composition	Purity	$8.7 \cdot 10^{-7}$ kg/mol	
	Molar mass	$3.3 \cdot 10^{-7}$ kg/mol	
	Quadrature Sum	$9.3 \cdot 10^{-7}$ kg/mol	23
Radius from speed of sound in Ar	Temperature	$1.5 \cdot 10^{-9}$ m	
	Pressure	$1.6 \cdot 10^{-10}$ m	
	Gas Composition	$4.1 \cdot 10^{-9}$ m	
	Frequency fitting	$4.9 \cdot 10^{-7}$ m	
	Regression	$1.7 \cdot 10^{-6}$ m	
	Equation of State	$2.3 \cdot 10^{-6}$ m	
	Dispersion of modes	$2.9 \cdot 10^{-6}$ m	
	Quadrature Sum	$4.2 \cdot 10^{-6}$ m	88
Frequency fitting		$7.6 \cdot 10^{-3}$ Hz	0.69
Dispersion of modes		$5.3 \cdot 10^{-3}$ m·s^{-1}	13
Quadrature Sum of all contributions to w_{exp}			92
$10^6 \cdot U_r(w_{exp})$ ($k = 2$)			180

Squared speed of sound data $w^2(p,T)$ have been fitted to the standard form of the acoustic virial equation as an expansion series of pressure p at each experimental temperature T as:

$$w^2\left(p,T\right) = A_0\left(T\right) + A_1\left(T\right)p + A_2\left(T\right)p^2 + A_3\left(T\right)p^3 + A_4\left(T\right)p^4 + A_5\left(T\right)p^5 \qquad (4)$$

providing that: (i) the residuals of the regression are randomly distributed within the above specified expanded ($k = 2$) uncertainty of the speed of sound, as it is shown in Figure 4; and (ii) the fitting parameters A_i, which are given in Table 7, are significant, i.e., their expanded ($k = 2$) uncertainties evaluated following the Monte Carlo method [42] are at least one order of magnitude lower than the parameters themselves.

(a)

(b)
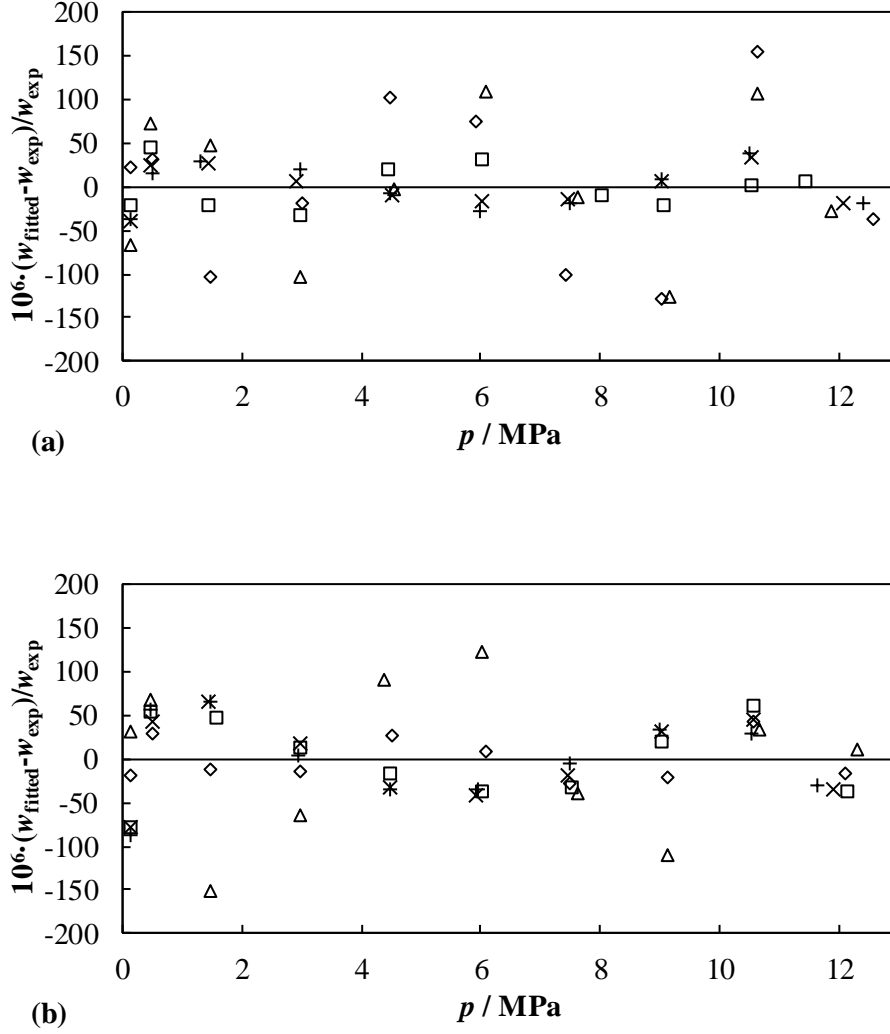
Figure 4. Residual plots $\Delta w = (w_{fitted} - w_{exp})/w_{exp}$ from the values regressed to Eq. (4) as a function of the pressure for: a) the 11 M synthetic natural gas and b) the H_2-enriched natural gas mixtures, at temperatures $T = \triangle$ 260 K, $\diamondsuit$ 273.16 K, $\square$ 300 K, $\times$ 325 K, $+$ 350 K.

Then, it is concluded that a polynomial of third order is required for all the isotherms except from the isotherms at $T = (260$ and $273.16)$ K for the 11M synthetic mixture, where a polynomial of fifth and a fourth order, respectively is needed. This approach results in relative residuals not higher than 150 parts in 10^6 in any case, with root mean squares below 90 parts in 10^6 for all the temperatures, which are within $U_r(w_{exp}) = (190$ and $180)$ parts in 10^6 for the 11 M synthetic and the H_2-enriched mixtures, respectively. We must remark that the estimated expanded ($k = 2$) uncertainties of $w^2(p,T)$ were used as weights in the fitting to Equation (4).

Table 7. Fitting parameters $A_i(T)$ of the squared speed of sound to Eq. (4), their corresponding expanded ($k = 2$) uncertainties determined by the Monte Carlo method and the root mean square (Δ_{RMS}) of the residuals of the fitting.

T / K	$A_0(T)$ / m²·s⁻²	$10^5 \cdot A_1(T)$ / m²·s⁻²·Pa⁻¹	$10^{12} \cdot A_2(T)$ / m²·s⁻²·Pa⁻²	$10^{19} \cdot A_3(T)$ / m²·s⁻²·Pa⁻³	$10^{26} \cdot A_4(T)$ / m²·s⁻²·Pa⁻⁴	$10^{32} \cdot A_5(T)$ / m²·s⁻²·Pa⁻⁵	Δ_{RMS} of residuals / ppm
			11 M synthetic natural gas				
260.00	154482 ± 16	−504.9 ± 3.6	216.0 ± 20.0	−249.0 ± 44.0	499.0 ± 41.0	−12.5 ± 1.3	79
273.16	161656 ± 17	−409.5 ± 2.5	58.6 ± 8.6	175.0 ± 11.0	39.5 ± 4.1		90
300.00	176102 ± 17	−297.4 ± 1.6	97.8 ± 3.4	125.7 ± 1.9			24
325.00	189192 ± 20	−216.9 ± 1.7	125.8 ± 3.6	69.4 ± 1.9			22
350.00	201951 ± 21	−148.4 ± 1.8	129.4 ± 3.6	41.2 ± 1.9			24
			H₂-enriched natural gas				
260.00	153355 ± 11	−329.70 ± 0.94	34.7 ± 1.9	216.7 ± 1.0			84
273.16	160679 ± 15	−282.6 ± 1.3	88.1 ± 2.6	144.2 ± 1.4			24
300.00	175179 ± 17	−191.6 ± 1.4	124.0 ± 2.9	72.3 ± 1.6			45
325.00	188296 ± 19	−119.2 ± 1.7	124.9 ± 3.6	42.8 ± 2.0			45
350.00	201091 ± 21	−58.9 ± 1.9	115.9 ± 4.1	28.1 ± 2.3			45

In addition, it can be demonstrated that [40]: (a) from A_0 the heat capacity ratio γ^{pg} as perfect-gas (zero pressure conditions) is obtained as $\gamma^{pg} = M \cdot A_0/(R \cdot T)$, whereby the molar isochoric heat capacity $C_{V,m}^{pg}$ as perfect-gas is $C_{V,m}^{pg} = R/(\gamma^{pg} - 1)$, and the molar isobaric heat capacity $C_{p,m}^{pg}$ as perfect-gas is $C_{p,m}^{pg} = \gamma^{pg} \cdot C_{V,m}^{pg}$, where M stands for the molar mass of the mixture and R for the molar gas constant; (b) from A_1 the second acoustic virial coefficient β_a is derived as $\beta_a = R \cdot T \cdot A_1/A_0$; and (c) from A_2 the third acoustic virial coefficient γ_a is determined as $\gamma_a = (R \cdot T)^2 \cdot A_2/A_0 + \beta_a \cdot B(T)$, where $B(T)$ stands for the second density virial coefficient. Table 8 shows the results of γ^{pg}, $C_{p,m}^{pg}$, β_a, and γ_a obtained from these regressions together with their relative expanded ($k = 2$) uncertainties, which includes the contributions from the uncertainty of temperature, molar mass, and fitted A_i parameters (note that after the redefinition of the kelvin, the uncertainty of R is zero [43,44]).

Table 8. Adiabatic coefficient γ^{pg}, isobaric heat capacity $C_{p,m}^{pg}$, acoustic second virial coefficient β_a, and acoustic third virial coefficient γ_a for the two natural gas mixtures analyzed in this work, with their corresponding relative expanded ($k = 2$) uncertainty, and comparison with AGA8-DC92 EoS [20,21] and GERG-2008 EoS [22,23]. The superscript pg indicates perfect-gas property.

$T\,/\,\text{K}$	γ^{pg}	$10^2 \cdot U_{\exp}(\gamma^{pg})$	$10^2 \cdot \Delta\gamma^{pg}_{\text{AGA}}{}^{(*)}$	$10^2 \cdot \Delta\gamma^{pg}_{\text{GERG}}{}^{(*)}$	$C_{p,m}^{pg}\,/$ $\text{J} \cdot \text{mol}^{-1} \cdot \text{K}^{-1}$	$10^2 \cdot U_{\exp}(C_{p,m}^{pg})$	$10^2 \cdot \Delta C_{p,m\text{AGA}}^{pg}{}^{(*)}$	$10^2 \cdot \Delta C_{p,m\text{GERG}}^{pg}{}^{(*)}$
				11 M synthetic natural gas				
260.00	1.30488	0.018	−0.056	−0.060	35.586	0.081	0.19	0.20
273.16	1.29970	0.018	−0.083	−0.086	36.057	0.083	0.28	0.29
300.00	1.28917	0.019	−0.052	−0.053	37.068	0.083	0.18	0.18
325.00	1.27845	0.019	−0.025	−0.026	38.174	0.087	0.092	0.093
350.00	1.26720	0.019	−0.016	−0.016	39.432	0.089	0.059	0.061
				H_2-enriched natural gas				
260.00	1.31914	0.012	−0.14	−0.15	34.367	0.053	0.45	0.46
273.16	1.31555	0.014	−0.087	−0.089	34.663	0.059	0.27	0.28
300.00	1.30595	0.014	−0.059	−0.059	35.491	0.061	0.19	0.19
325.00	1.29575	0.014	−0.057	−0.055	36.427	0.065	0.19	0.18
350.00	1.28496	0.014	−0.065	−0.063	37.492	0.067	0.23	0.22

	$10^7 \cdot \beta_a$ / m³·mol⁻¹	$10^2 \cdot U_{exp}(\beta_a)$	$10^2 \cdot \Delta\beta_{a,AGA}$ [*]	$10^2 \cdot \Delta\beta_{a,GERG}$ [*]	$10^{10} \cdot \gamma_a$ / (m³·mol⁻¹)²	$10^2 \cdot U_{exp}(\gamma_a)$	$10^2 \cdot \Delta\gamma_{a,AGA}$ [*]	$10^2 \cdot \Delta\gamma_{a,GERG}$ [*]
				11 M synthetic natural gas				
260.00	−706.5	0.71	1.6	2.2	113.4	5.3	42	45
273.16	−575.3	0.59	−4.4	−3.6	53.5	5.2	−30	−29
300.00	−421.3	0.52	−4.7	−3.5	54.8	2.2	−22	−21
325.00	−309.8	0.77	−4.0	−2.0	60.5	2.3	−8.7	−6.8
350.00	−213.9	1.2	−4.5	−1.3	60.9	2.5	−4.1	−1.1
				H_2-enriched natural gas				
260.00	−464.8	0.28	−7.6	−6.9	35.85	1.6	−47	−45
273.16	−399.4	0.45	−5.5	−4.6	47.52	1.8	−26	−25
300.00	−272.8	0.73	−4.8	−3.3	54.2	1.9	−9.8	−8.3
325.00	−171.0	1.4	−7.3	−4.7	53.5	2.6	−6.9	−5.1
350.00	−85.3	3.3	−15	−9.7	50.7	3.4	−8.5	−6.2

[*] $\Delta X_{EoS} = (X_{exp} − X_{EoS})/X_{EoS}$ with $X = \gamma^{pg}$, $C_{p,m}^{pg}$, β_a, γ_a; and EoS = AGA8-DC92 [20,21], GERG-2008 [22,23].

4. Discussion.

4.1 Speed of sound.
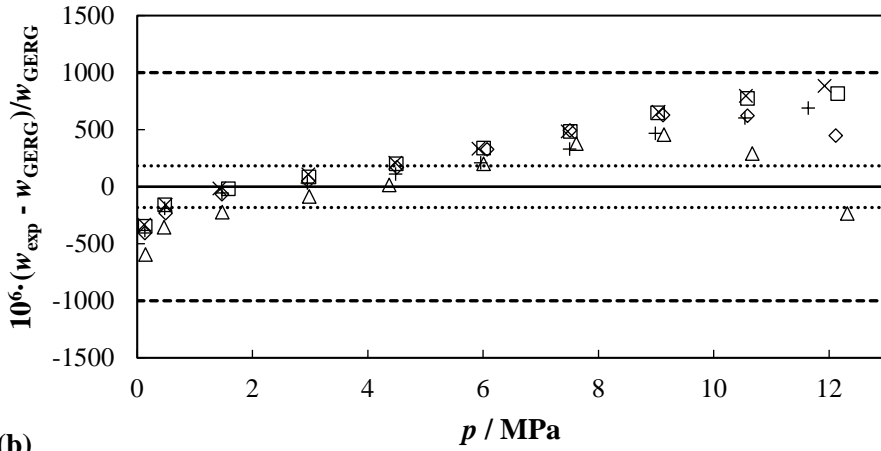
The relative deviations of the experimental speeds of sound w_{exp} determined in this research from those evaluated by the reference thermodynamic models used in the industry, AGA8-DC92 EoS [20,21] and GERG-2008 EoS [22,23], are given in Table 3 and 4 and depicted in Figures 5 and 6 for the 11 M synthetic natural gas and the H_2-enriched natural gas mixtures, respectively.

(a)

(b)
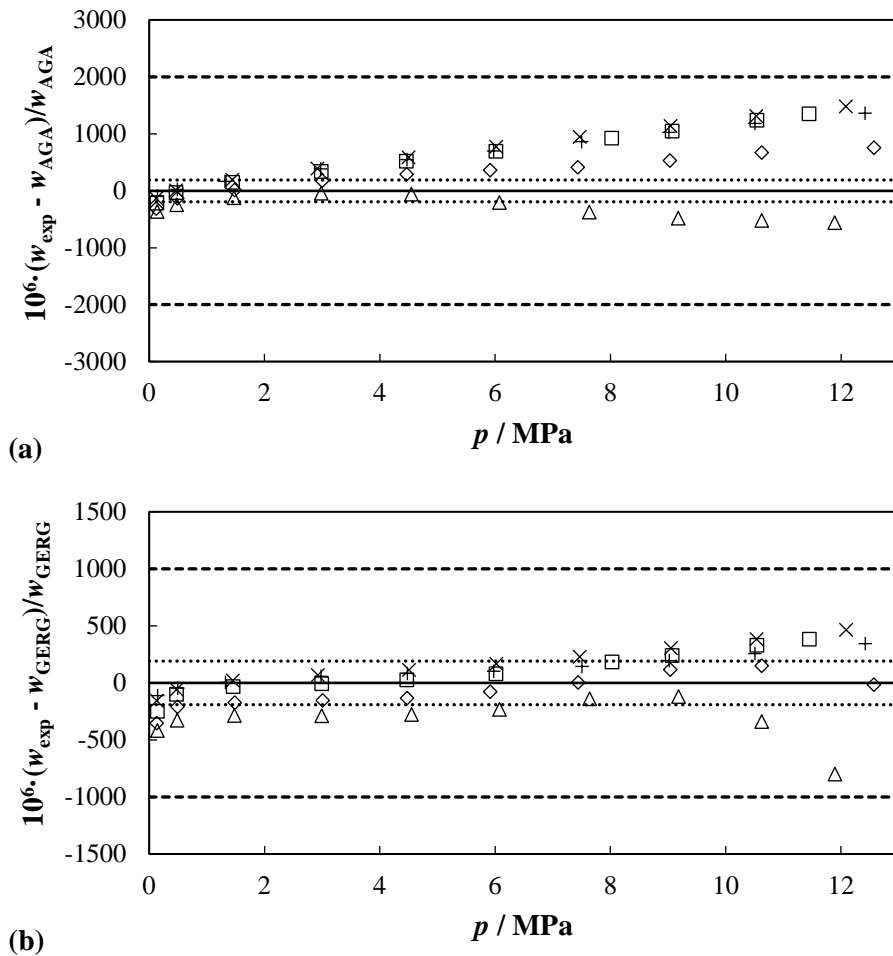
Figure 5. Relative deviations of experimental speed of sound $\Delta w = (w_{exp} - w_{EoS})/w_{EoS}$ from speed of sound values calculated from the reference models: a) AGA8-DC92 EoS [20,21] and b) GERG-2008 EoS [22,23] as function of pressure for the 11 M synthetic natural gas mixture at temperatures T = △ 260 K, ◇ 273.16 K, □ 300 K, × 325 K, + 350 K. The dotted lines depict the expanded ($k = 2$) uncertainty of the experimental speed of sound. The dashed lines represent the uncertainty of the reference models.
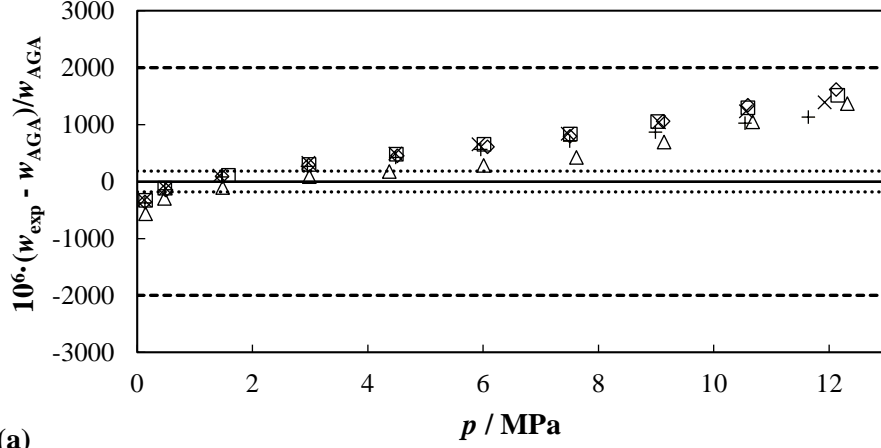
(a)

(b)

Figure 6. Relative deviations of experimental speed of sound $\Delta w = (w_{exp} - w_{EoS})/w_{EoS}$ from speed of sound values calculated from the reference models: a) AGA8-DC92 EoS [20,21] and b) GERG-2008 EoS [22,23] as function of pressure for the H_2-enriched natural gas mixture at temperatures $T = \triangle$ 260 K, $\Diamond$ 273 K, $\square$ 300 K, $\times$ 325 K, $+$ 350 K. The dotted lines depict the expanded ($k = 2$) uncertainty of the experimental speed of sound. The dashed lines represent the uncertainty of the reference models.

At all experimental conditions, the deviations of the speed of sound remain within the limit stated by the expanded ($k = 2$) uncertainty in the speed of sound of both models for natural gas-like mixtures, namely $U_{AGA8-DC92}(w) = 2000$ parts in 10^6 (0.2 %) and $U_{GERG-2008}(w) = 1000$ parts in 10^6 (0.1 %). However, the differences are only explained within the experimental expanded ($k = 2$) uncertainty $U_r(w_{exp})$ for pressures below (4 and 9) MPa with regards to the AGA and GERG equations, respectively, for the 11 M mixture and below (3 and 5) MPa with respect to the AGA and GERG models, respectively, for the H_2-enriched mixture.

The comparison between both mixtures reveals that adding a nominal hydrogen mole percentage of 3 % results in increasing deviations towards higher pressures, with a nearly linear trend which is fairly independent of temperature. This effect is particularly noticeable for the GERG-2008 EoS [22,23] at all the studied isotherms and for the AGA8-DC92 EoS [20,21] at the lowest temperature of 260 K.

Table 9 lists overall indicators of the predicting capability of the two models: the average absolute deviations Δ_{AAD} for the two mixtures, together with the root mean square Δ_{RMS}, the bias Δ_{Bias}, and the maximum deviation Δ_{Max}, which also serve for further comparison with other studies on speed of sound.

Table 9. Statistical analysis of the speed of sound data with respect to AGA8-DC92 EoS [20,21] and GERG-2008 EoS [22,23] for the two natural gas mixtures studied in this work. Δ_{AAD} = average absolute relative deviation, Δ_{Bias} = average relative deviation, Δ_{RMS} = root mean square relative deviation, Δ_{Max} = maximum relative deviation.

	$10^2 \cdot$ (Experimental vs AGA)				$10^2 \cdot$ (Experimental vs GERG)			
	Δ_{AAD}	Δ_{Bias}	Δ_{RMS}	Δ_{Max}	Δ_{AAD}	Δ_{Bias}	Δ_{RMS}	Δ_{Max}
11 M synthetic natural gas	0.053	0.037	0.064	0.11	0.019	−0.0014	0.023	0.047
H$_2$-enriched natural gas	0.061	0.050	0.075	0.14	0.034	0.019	0.041	0.072

As it can be seen, the discrepancies are twice higher for the AGA8-DC92 EoS [20,21] than the GERG-2008 EoS [22,23] with reference to the two mixtures at the same states, although the impact of adding hydrogen is twice more pronounced for the GERG-2008 EoS [22,23] than the AGA8-DC92 EoS [20,21], with Δ_{AAD} for the AGA equation that ranges from (0.05 to 0.06) %, in contrast with Δ_{AAD} for the GERG equation from (0.02 up to 0.04) %. The reason for this relative underperformance of the GERG-2008 EoS [22,23] for hydrogen-containing mixtures could be the non-existent departure function due to the absence of accurate and wide-range experimental data able to model the binary interactions between hydrogen and such important components for natural gas-like mixtures, as nitrogen, carbon dioxide, ethane, propane and butane, and of fitted

combining rules with pentane. In addition to the existing development of a binary specific departure function with methane, the EoS are still worthwhile to be improved, so there is a need for consolidated experimental data that can be employed for the building of departure functions, as supported by this paper and discussed elsewhere [41,45].

4.2 Perfect-gas heat capacities and acoustic virial coefficients.

Table 8 compares the experimental heat capacity ratios γ^{pg} and the molar isobaric heat capacities as perfect-gas $C_{\mathrm{p,m}}^{\mathrm{pg}}$ with calculated values from the reference AGA8-DC92 EoS [20,21] and the GERG-2008 EoS [22,23]. The hydrogen content of 3 % to a natural gas mixture decreases the $C_{\mathrm{p,m}}^{\mathrm{pg}}$ between (3.4 up to 4.9) % as the temperature increases.

Both equations of state yield nearly the same heat capacity values as perfect-gas at every temperature and successfully represent the experimental results, with a resulting $\Delta_{\mathrm{AAD}} = 0.16$ % for the 11 M synthetic mixture and a $\Delta_{\mathrm{AAD}} = 0.27$ % for the H_2-enriched mixture, respectively, well below the expanded ($k = 2$) model uncertainty $U_{\mathrm{EoS}}(C_{\mathrm{p,m}}^{\mathrm{pg}}) = 1.0$ %.

However, when comparing with the 11 M synthetic mixture only at the isotherms $T = (325$ and $350)$ K, the relative differences are within the mean experimental expanded ($k = 2$) uncertainty $U_{\mathrm{exp}}(C_{\mathrm{p,m}}^{\mathrm{pg}}) = 0.085$ %. By contrast, with respect to the H_2-enriched mixture, the disagreement is almost twofold at all temperatures, always beyond the corresponding mean experimental expanded ($k = 2$) uncertainty $U_{\mathrm{exp}}(C_{\mathrm{p,m}}^{\mathrm{pg}}) = 0.061$ %.

Table 8 also lists the relative deviations of the experimental second acoustic virial coefficient β_{a} and third acoustic virial coefficient γ_{a} from the estimations of the AGA8-DC92 EoS [20,21] and the GERG-2008 EoS [22,23]. Both models overpredict the experimental results at all temperatures with the exception of the lowest isotherm $T = 260$ K in the 11 M synthetic mixture. Regarding β_{a}, the relative differences can be as much as halved when compared to the GERG-2008 EoS [22,23] than when compared to the AGA8-DC92 [20,21] for both mixtures, worsening the agreement from an $\Delta_{\mathrm{AAD}} = 2.5$ % in the 11 M synthetic mixture up to $\Delta_{\mathrm{AAD}} = 5.8$ % in the H_2-enriched mixture with respect to the GERG-2008 EoS [22,23].

With respect to γ_a, discrepancies raise one order of magnitude more than those of β_a, but show a decrease with increasing temperatures. This coefficient seems to be insensitive to hydrogen in the natural gas at the studied concentration. Note that, in any case, the relative deviations are far beyond the corresponding mean experimental expanded ($k = 2$) uncertainties $U_{exp}(\beta_a) = 1.0$ % and $U_{exp}(\gamma_a) = 2.9$ %.

5. Conclusions.

We report new accurate experimental speed of sound data $w_{exp}(p,T,\bar{x})$ at pressures between $p = $ (0.1 up to 13) MPa and temperatures $T = (260$ to $350)$ K of an 11 component synthetic natural gas mixture and a H$_2$-enriched natural gas with a nominal molar percentage $x_{H_2} = 3$ %. Heat capacity ratio γ^{pg}, perfect-gas heat capacity $C_{p,m}^{pg}$, second β_a, and third γ_a acoustic virial coefficients have been derived from the speed of sound values.

Taking into account the speed of sound $w_{exp}(p,T,\bar{x})$, this study reveals that: (i) AGA8-DC92 EoS [20,21] performs worse than GERG-2008 EoS [22,23], in agreement with other authors [18]; (ii) all the relative deviations fall within the expanded ($k = 2$) uncertainty of each model, $U_{AGA8-DC92}(w)$ = 0.2 % and $U_{GERG-2008}(w) = 0.1$ %, respectively; (iii) however, there is a clear increment in the relative differences for the H$_2$-containing natural gas mixture compared to the synthetic natural gas, mainly at low temperatures for the lower pressures, and conversely at high temperatures for the higher pressures, which are in the limit of the model uncertainty for the latter case. Analogous results apply to $C_{p,m}^{pg}$, β_a, and γ_a.

Considering that most of the relative discrepancies also are beyond our experimental expanded (k = 2) uncertainty $U_r(w_{exp}) \sim 0.02$ %, $U_{exp}(C_{p,m}^{pg}) \sim 0.07$ %, $U_{exp}(\beta_a) = 1.0$ % and $U_{exp}(\gamma_a) = 2.9$ %, we conclude that there is still a need for improvement of the current thermodynamic enhance their performance on hydrogen-containing mixtures. This objective can be approached when further accurate and extensive data sets of binary mixtures of hydrogen with nitrogen, carbon dioxide, and other hydrocarbons apart from methane have become available.

References

[1]   M. Wietschel, M. Ball, The hydrogen economy: Opportunities and challenges, Cambridge University Press, Cambridge, 2009. https://doi.org/10.1017/CBO9780511635359.

[2]   M. Qadrdan, M. Abeysekera, J. Wu, N. Jenkins, B. Winter, The future of gas networks. The role of gas networks in a low carbon energy system, Springer International Publishing, Cham, 2020. https://doi.org/10.1007/978-3-319-66784-3.

[3]   E.A. Polman, H. de Laat, J. Stappenbelt, P. Peereboom, W. Bouwman, B. de Bruin, C. Pulles, M. Hagen, Reduction of CO2 emissions by adding hydrogen to natural gas. Report no. IE/020726/Pln, Gastec NV, Apeldoorn, The Netherlands, 2003.

[4]   M.W. Melaina, O. Antonia, M. Penev, Blending Hydrogen into Natural Gas Pipeline Networks: A Review of Key Issues. Technical Report NREL/TP-5600-51995, National Renewabler Energy Laboratory, Golden, CO (United States), 2013. https://doi.org/10.2172/1068610.

[5]   M. Thema, F. Bauer, M. Sterner, Power-to-Gas: Electrolysis and methanation status review, Renew. Sustain. Energy Rev. 112 (2019) 775–787. https://doi.org/10.1016/j.rser.2019.06.030.

[6]   Stanford Research Systems, SRS Technical Note, A Comparison Between Stanford Research Systems BGA244 Binary Gas Analyzer and Inficon Composer Elite Gas Concentration Monitor, (2020).

https://www.thinksrs.com/downloads/pdfs/applicationnotes/BGA244 vs Composer Elite.pdf.

[7] L. Zipser, F. Wächter, H. Franke, Acoustic gas sensors using airborne sound properties, Sensors Actuators, B Chem. 68 (2000) 162–167. https://doi.org/10.1016/S0925-4005(00)00478-0.

[8] A. Elshahomi, C. Lu, G. Michal, X. Liu, A. Godbole, P. Venton, Decompression wave speed in CO2 mixtures: CFD modelling with the GERG-2008 equation of state, Appl. Energy. 140 (2015) 20–32. https://doi.org/10.1016/j.apenergy.2014.11.054.

[9] B. Liu, X. Liu, C. Lu, A. Godbole, G. Michal, L. Teng, Decompression of hydrogen—natural gas mixtures in high-pressure pipelines: CFD modelling using different equations of state, Int. J. Hydrogen Energy. 44 (2019) 7428–7437. https://doi.org/10.1016/j.ijhydene.2019.01.221.

[10] National Measurement System, Good Practice Guide - The Calibration of Flow Meters, 2017.

[11] M. Castier, Modeling and simulation of supersonic gas separations, J. Nat. Gas Sci. Eng. 18 (2014) 304–311. https://doi.org/10.1016/j.jngse.2014.03.014.

[12] J.L. de Medeiros, L. de Oliveira Arinelli, A.M. Teixeira, O. de Q.F. Araújo, Offshore Processing of CO2-Rich Natural Gas with Supersonic Separator, Springer International Publishing, Cham, 2019. https://doi.org/10.1007/978-3-030-04006-2.

[13] M.B. Ewing, A.R.H. Goodwin, Speeds of sound in a natural gas of specified composition at the temperature 255 k and pressures in the range 64 kpa to 6.1 MPa, J. Chem. Thermodyn. 25 (1993) 1503–1511. https://doi.org/10.1006/jcht.1993.1150.

[14] P. Labes, J.L. Daridon, B. Lagourette, H. Saint-Guirons, Measurement and prediction of ultrasonic speed under high pressure in natural gases, Int. J. Thermophys. 15 (1994) 803–819. https://doi.org/10.1007/BF01447096.

[15] B.A. Younglove, N. V. Frederick, Sound speed measurements on gas mixtures of natural gas components using a cylindrical resonator, Int. J. Thermophys. 11 (1990) 897–910. https://doi.org/10.1007/BF00503582.

[16]   B.A. Younglove, N. V Frederick, R.D. McCarty, Speed of sound data and related models for mixtures of natural gas constituents, Gaithersburg, MD, 1993. https://doi.org/10.6028/NIST.MONO.178.

[17]   M.F. Costa Gomes, J.P.M. Trusler, The speed of sound in two methane-rich gas mixtures at temperatures between 250 K and 350 K and at pressures up to 20 MPa, J. Chem. Thermodyn. 30 (1998) 1121–1129. https://doi.org/10.1006/jcht.1998.0378.

[18]   P. Ahmadi, A. Chapoy, B. Tohidi, Density, speed of sound and derived thermodynamic properties of a synthetic natural gas, J. Nat. Gas Sci. Eng. 40 (2017) 249–266. https://doi.org/10.1016/j.jngse.2017.02.009.

[19]   R. Hernández-Gómez, D. Tuma, D. Lozano-Martín, C.R. Chamorro, Accurate experimental (p, ρ, T) data of natural gas mixtures for the assessment of reference equations of state when dealing with hydrogen-enriched natural gas, Int. J. Hydrogen Energy. 43 (2018) 21983–21998. https://doi.org/10.1016/j.ijhydene.2018.10.027.

[20]   Transmission Measurement Committee, AGA Report No. 8 Part 1 Thermodynamic Properties of Natural Gas and Related Gases DETAIL and GROSS Equations of State, Washington DC, 2017.

[21]   International Organization for Standardization, ISO 20765-1 Natural gas — Calculation of thermodynamic properties — Part 1: Gas phase properties for transmission and distribution applications, Genève, 2005.

[22]   O. Kunz, R. Klimeck, W. Wagner, M. Jaeschke, GERG Technical Monograph 15 The GERG-2004 wide-range equation of state for natural gases and other mixtures, Düsseldorf, 2007.

[23]   O. Kunz, W. Wagner, The GERG-2008 Wide-Range Equation of State for Natural Gases and Other Mixtures: An Expansion of GERG-2004, J. Chem. Eng. Data. 57 (2012) 3032–3091. https://doi.org/10.1021/je300655b.

[24]   J.P.M. Trusler, Physical Acoustics and Metrology of Fluids, CRC Press, Taylor & Francis Group, 1991.

[25]   E.W. Lemmon, I.H. Bell, M.L. Huber, M.O. McLinden, NIST Standard Reference

Database 23: Reference Fluid Thermodynamic and Transport Properties-REFPROP, Version 10.0, National Institute of Standards and Technology, (2018) 135. https://doi.org/https://doi.org/10.18434/T4/1502528.

[26] International Organization for Standardization, ISO 6142-1 Gas analysis — Preparation of calibration gas mixtures — Part 1: Gravimetric method for Class I mixtures, Genève, 2014.

[27] International Organization for Standardization, ISO 20765-2 Natural gas — Calculation of thermodynamic properties — Part 2: Single-phase properties (gas, liquid, and dense fluid) for extended ranges of application, Genève, 2013.

[28] D. Lozano-Martín, A. Rojo, M.C. Martín, D. Vega-Maza, J.J. Segovia, Speeds of sound for (CH4 + He) mixtures from p = (0.5 to 20) MPa at T = (273.16 to 375) K, J. Chem. Thermodyn. 139 (2019). https://doi.org/10.1016/j.jct.2019.07.011.

[29] F.J. Pérez-Sanz, J.J. Segovia, M.C. Martín, D. Del Campo, M.A. Villamañán, Speeds of sound in (0.95 N2 + 0.05 CO and 0.9 N2 + 0.1 CO) gas mixtures at T = (273 and 325) K and pressure up to 10 MPa, J. Chem. Thermodyn. 79 (2014) 224–229. https://doi.org/10.1016/j.jct.2014.07.022.

[30] C. Tegeler, R. Span, W. Wagner, A New Equation of State for Argon Covering the Fluid Region for Temperatures From the Melting Line to 700 K at Pressures up to 1000 MPa, J. Phys. Chem. Ref. Data. 28 (1999) 779–850. https://doi.org/10.1063/1.556037.

[31] H. Preston-Thomas, The International temperature scale of 1990 (ITS-90), Metrologia. 27 (1990) 3–10. https://doi.org/10.1088/0026-1394/27/1/002.

[32] M.R. Moldover, J.B. Mehl, M. Greenspan, Gas-filled spherical resonators: Theory and experiment, J. Acoust. Soc. Am. 79 (1986) 253–272. https://doi.org/10.1121/1.393566.

[33] J.B. Mehl, Spherical acoustic resonator: Effects of shell motion, J. Acoust. Soc. Am. 78 (1985) 782–788. https://doi.org/10.1121/1.392448.

[34] K.A. Gillis, H. Lin, M.R. Moldover, Perturbations From Ducts on the Modes of Acoustic Thermometers, J. Res. Natl. Inst. Stand. Technol. 114 (2009) 263. https://doi.org/10.6028/jres.114.019.

[35]   J.B. Mehl, Acoustic eigenvalues of a quasispherical resonator: Second order shape

         perturbation theory for arbitrary modes, J. Res. Natl. Inst. Stand. Technol. 112 (2007)

         163–173. https://doi.org/10.6028/jres.112.013.

[36]   D. Lozano-Martín, J.J. Segovia, M.C. Martín, T. Fernández-Vicente, D. del Campo,

         Speeds of sound for a biogas mixture CH4 + N2 + CO2 + CO from p = (1–12) MPa at

         T = (273, 300 and 325) K measured with a spherical resonator, J. Chem. Thermodyn.

         102 (2016) 348–356. https://doi.org/10.1016/j.jct.2016.07.033.

[37]   H.M. Ledbetter, W.F. Weston, E.R. Naimon, Low-temperature elastic properties of four

         austenitic stainless steels, J. Appl. Phys. 46 (1975) 3855–3860.

         https://doi.org/10.1063/1.322182.

[38]   Cryogenic technologies group, Material properties: 304 stainless (UNS S30400), (2020).

         https://trc.nist.gov/cryogenics/materials/304Stainless/304Stainless_rev.htm.

[39]   CryoSoft, Solid materials database, (2020).

         https://supermagnet.sourceforge.io/solids/MetallicAlloys/SS304/rep/AISI304.pdf.

[40]   F.J. Pérez-Sanz, M.C. Martín, C.R. Chamorro, T. Fernández-Vicente, J.J. Segovia, Heat

         capacities and acoustic virial coefficients for a synthetic coal mine methane mixture by

         speed of sound measurements at T = (273.16 and 250.00) K, J. Chem. Thermodyn. 97

         (2016) 137–141. https://doi.org/10.1016/j.jct.2016.01.020.

[41]   D. Lozano-Martín, M.C. Martín, C.R. Chamorro, D. Tuma, J.J. Segovia, Speed of sound

         for three binary (CH4 + H2) mixtures from p = (0.5 up to 20) MPa at T = (273.16 to 375)

         K, Int. J. Hydrogen Energy. 45 (2020) 4765–4783.

         https://doi.org/10.1016/j.ijhydene.2019.12.012.

[42]   Joint Committee for Guides in Metrology, Evaluation of measurement data —

         Supplement 1 to the "Guide to the expression of uncertainty in measurement" —

         Propagation of distributions using a Monte Carlo method, Sèvres, 2008.

[43]   J.J. Segovia, D. Lozano-Martín, M.C. Martín, C.R. Chamorro, M.A. Villamañán, E.

         Pérez, C. García Izquierdo, D. Del Campo, Updated determination of the molar gas

         constant R by acoustic measurements in argon at UVa-CEM, Metrologia. 54 (2017)

663–673. https://doi.org/10.1088/1681-7575/aa7c47.

[44]   J. Fischer, B. Fellmuth, C. Gaiser, T. Zandt, L. Pitre, F. Sparasci, M.D. Plimmer, M. De

Podesta, R. Underwood, G. Sutton, G. Machin, R.M. Gavioso, D. Madonna Ripa, P.P.M.

Steur, J. Qu, X.J. Feng, J. Zhang, M.R. Moldover, S.P. Benz, D.R. White, L. Gianfrani,

A. Castrillo, L. Moretti, B. Darquié, E. Moufarej, C. Daussy, S. Briaudeau, O. Kozlova,

L. Risegari, J.J. Segovia, M.C. Martin, D. Del Campo, The Boltzmann project,

Metrologia. 55 (2018) R1–R20. https://doi.org/10.1088/1681-7575/aaa790.

[45]   R. Hernández-Gómez, D. Tuma, E. Pérez, C.R. Chamorro, Accurate Experimental (p, ρ,

and T) Data for the Introduction of Hydrogen into the Natural Gas Grid (II):

Thermodynamic Characterization of the Methane-Hydrogen Binary System from 240 to

350 K and Pressures up to 20 MPa, J. Chem. Eng. Data. 63 (2018) 1613–1630.

https://doi.org/10.1021/acs.jced.7b01125.